JOURNAL OF AIRCRAFT
Vol. 38, No. 5, September–October 2001

Flight Testing the Parachute System for the Space Station Crew Return Vehicle

Ricardo A. Machín,* Christie S. Iacomini,† Chris J. Cerimele,‡ and Jenny M. Stein§
NASA Johnson Space Center, Houston, Texas 77058

NASA has developed and tested a large parafoil for use in landing the International Space Station crew return vehicle. A series of tests using low-velocity airdrop pallets and prototype lifting bodies flights has demonstrated that the parafoil recovery system is a viable option for safely landing a crewed vehicle. The aerodynamic characteristics of the parafoil system have been determined through a series of flight-test maneuvers and subsequently successfully modeled using an eight-degree-of-freedom simulation program. An introduction to the requirements for the crew return vehicle, a description of the parafoil system, an overview of the testing performed including several significant findings, a description of the techniques used to assess the aerodynamic performance of the parafoil system, and a discussion of the simulation of the parafoil system are presented.

Nomenclature

AR	=	aspect ratio
b	=	parafoil span
C_L, C_D	=	lift and drag coefficients
$Cm_{c/4}$	=	parafoil system pitching moment coefficient about $c/4$
Cn_r	=	yawing moment due to yaw rate
$Cn_{\delta f}$	=	yawing moment due to control line deflection difference between left and right flaps
c	=	parafoil chord
$c/4$	=	quarter chord point on the parafoil keel
HR	=	velocity vector heading rate
HR_{wc}	=	wind-corrected heading rate
$\bar{q}$	=	dynamic pressure
RA, θ_r	=	parafoil rigging angle (X_{pf} to parafoil keel)
R/b	=	line length ratio (average suspension line length divided by span)
S	=	parafoil reference area
t	=	time, where $t1$ is time at first data point and $t2$ time at second data point
Vh_{wc}	=	wind-corrected horizontal velocity
V_{tot}	=	total velocity
V_w	=	wind velocity
V_x	=	east velocity
V_y	=	north velocity
V_z	=	vertical velocity
W_{pf}	=	weight of the parafoil system, including rigging, but not payload
W_{sys}	=	weight of the parafoil system and payload
W/S	=	wing loading (payload weight divided by parafoil area)
X_{cg}, Y_{cg}	=	distance from the confluence to the parafoil system c.g. in parafoil coordinates
X_{PL}	=	payload body axis parallel to payload's bottom surface
X_{pf}, Z_{pf}	=	parafoil coordinate system, Z axis originating at the confluence point with $-Z$ extending up through $c/4$
$Z_{c/4}$	=	distance from the confluence to the $c/4$
α	=	parafoil angle of attack relative to keel
α_{PL}	=	payload angle of attack relative to X_{PL}
γ	=	wind-corrected flight-path angle (V_{wc} to horizon)
δ_f	=	control line deflection delta
θ	=	parafoil pitch angle (X_{pf} to horizon)
ρ	=	atmospheric density
ϕ_w	=	direction of the wind measured from the north, that is, wind is coming from ϕ_w
$\Psi_b^{\&}$	=	body yaw rate

Received 20 February 2000; revision received 10 February 2001; accepted for publication 13 February 2001. Copyright © 2001 by the American Institute of Aeronautics and Astronautics, Inc. No copyright is asserted in the United States under Title 17, U.S. Code. The U.S. Government has a royalty-free license to exercise all rights under the copyright claimed herein for Governmental purposes. All other rights are reserved by the copyright owner.

*X-38 Parachute Flight Test Director, Aeroscience and Flight Mechanics Division, Mail Code EG3. Member AIAA.

†Aerospace Engineer, Aeroscience and Flight Mechanics Division, Mail Code EG5. Member AIAA.

‡Deputy Branch Chief, Aeroscience and Flight Mechanics Division, Mail Code EG5. Member AIAA.

§X-38 Parachute System Lead, Advanced Development Division, Mail Code EX. Member AIAA.

Introduction

ASSEMBLY of the International Space Station has begun in earnest with the launch of the first element in November of 1998. Early in the planning for the International Space Station, it was determined that no crew would be placed in residence on the station without an autonomous method of returning to Earth. Initially this criterion will be met temporarily with Russian Soyuz spacecraft. Limitations of the Soyuz spacecraft such as limited number and size of crew members and the limited life of reaction control system fuel dictate a more robust solution to the requirement. To meet the longer-term needs of the station, NASA set out to build an operational crew return vehicle (CRV). This vehicle will be capable of returning seven crew members to Earth when the shuttle is not present at the station. Typical scenarios for use of the CRV include crew member illness or injury, catastrophe aboard the station (such as fire or micrometeoroid impact), or the inability to resupply the station due to a space shuttle problem.

In the late 1980s, when the CRV requirement was first identified and a project office to define its cost was established at the NASA Johnson Space Center, a development cost of $2 billion was projected. The high cost resulted in a decision to postpone CRV development until after the main assembly of the station was under way. In 1995, a team at NASA Johnson Space Center devised an alternate approach to produce a lower cost CRV using prototype vehicles flown in an unpiloted mode to test the critical technologies required. This prototype program was subsequently denoted the X-38.

The X-38 program calls for a number of different test vehicles, based on the Air Force X-24A lifting body design, each of increasing technical complexity, aimed at sequentially proving more and more of the technologies required for the operational CRV.[1] The program to date has extensively utilized the low-cost option of pallet drops from C-130 aircraft to develop the requisite parachute systems. Four specific vehicles, V-131, -132, -133, and -201 have been defined to advance the technologies nearer to the operational

CRV requirements in a stepwise fashion. The 130 series are all atmospheric vehicles to be released in-flight from the NASA B-52, whereas vehicle 201 is to be placed in orbit by the space shuttle and returned autonomously to demonstrate the full compliment of technologies required for the CRV. V-201 is currently manifested to fly on space shuttle mission STS-107 in February of 2002.

A primary goal of the CRV is to ensure that two prepared dry land touchdown sites can be guaranteed to be reached after no more than 4.5 h following an anytime departure from the space station. Whereas choosing the lifting body shape helps assure this goal by virtue of its cross range ability during reentry, a lifting body at the wing loading being considered for crew return would require landing speeds up to 250 kn (129 m/s), a speed that requires very long runways and intensive pilot training or complex automated landing systems. Early in the evolution of the X-38 program, a rectangular ram-air lifting parachute (parafoil) was chosen as the primary recovery system. This decision was driven by a number of factors. The parafoil can be steered to penetrate ground winds and assure within some small error a known orientation for touchdown allowing for a more achievable design of the crew couches. The lifting body shape is known to be roll sensitive to crab angle at touchdown, whereas a round chute would not guarantee a known orientation at touchdown, it was felt that a parafoil could be used to minimize crab angle at touchdown. A parafoil can be placed into a high-lift configuration and even flared at touchdown to achieve less than 20 ft/s (6.1 m/s) rate of descent at touchdown; an equivalent round chute system was estimated to weigh at least 30% more and take more volume than a parafoil system.

The 130 vehicle series have been built such that they can interface with the NASA B-52, be transported to altitude, and then be released. There are currently three atmospheric lifting body test vehicles planned for X-38. V-131 is the original vehicle design (sized for four humans) with the vehicle aerosurfaces pinned in place. V-132 is the original vehicle design with articulated control surfaces. V-133 is the current design sized for seven humans (120% size of the original design and a modified outer mold line) with articulated control surfaces.

This paper is a synthesis of three papers presented at the 15th Confederation of European Aerospace Societies/AIAA Aerodynamic Decelerator Systems Conference in June 1999.[2–4] At the same conference, Smith and Bennett[5] presented a more detailed description of the parachutes for both the primary and backup system; therefore, only a general overview of the recovery system will be presented herein. A brief history of the testing performed follows, and finally a discussion of the extraction of the parafoil performance characteristics and their application in a simulation of the parafoil system will be engaged.

Primary Recovery System Description

For the atmospheric development lifting bodies, the primary recovery system consists of three main components: a mortar deployed pilot chute, an initial decelerator drogue parachute, and the parafoil itself. The primary recovery system is initiated by the jettison of the parafoil compartment hatch by vehicle initiated actuators. The primary mortar is fired 1 s later, and the pilot parachute deployed. The mortar and pilot parachute are identical to that used on the space shuttle drag parachute system, with the exception that the pilot parachute has been strengthened by United Space Booster, Inc., at NASA Kennedy Space Center [the nominal initial dynamic pressure for deployment of the main system is 260 lb/ft^2 (12.5 Kpa)]. The pilot parachute, built by Irvin Aerospace, extracts and deploys the drogue parachute, a 60-ft-diam (18.3 m) ringslot, from the aft storage compartment. The drogue, built by Pioneer Aerospace Corporation, is initially attached by a Y bridle two-point attach system at the aft end of the vehicle and is reefed to less than 15% of its full open drag area. Disreefing is achieved using redundant predetermined time delay pencil cutters. Following first-stage inflation, the drogue is repositioned using vehicle-mounted pyrotechnic strap cutters (which are initiated by the onboard flight control computer) to a four-point attach system that straddles the main parafoil compartment. Reposition orients the vehicle such that subsequent disreef loads are aligned with the vehicle Z axis. After disreefing (the main drogue has three reefing stages) to full open and stabilizing the vehicle from the dynamics associated with repositioning, the drogue is released at 15,000-ft (4,570 m) mean sea level (msl) by vehicle pyrotechnic strap cutters (again initiated by the onboard flight control computer). A deployment line attached to one of the four legs of the drogue extracts and deploys the primary parafoil system.

The primary parafoil, built by Pioneer Aerospace Corporation, consists of a 31 cell rectangular planform canopy with a span of $121\frac{1}{2}$ ft (37 m), a chord of 45 ft (13.7 m), and planform area of 5468 ft^2 (508 m^2) using a Clark-Y airfoil section. The parafoil is reefed in five stages by a technique referred to as midspan reefing. In first stage, the current parafoil design has only 11 cells exposed to the freestream with the remaining interior 20 cells reefed closed spanwise by a system of reefing lines along the lower surface of the parafoil. The reefed stages are released from the leading edge back to the trailing edge by redundant predetermined time delay pencil cutters that are stored in pockets on the suspension lines and armed when the parafoil is extracted from the deployment bag. The four disreef times have been balanced achieving various objectives: controlling the opening loads, allowing for the inflation of the additional cells introduced in each new stage of the parafoil, damping of any dynamics associated with inflation and stage disreefing, and the desire to achieve a full open canopy as quickly as possible. The parafoil is fully disreefed in less than 25 s from the time the drogue is released, during which time the vehicle looses approximately 2000 ft (610 m) in altitude. The parafoil is joined to the vehicle four-point attach slings via a metal confluence fitting, which is held closed during deployment and disreefing, effectively creating a single-point confluence. The confluence fitting is released (using predetermined timed pencil cutters) after the parafoil has disreefed to full open. Once released, the confluence fitting separates, and the four attach slings along with their associated crossover slings provide an attach system that effectively couples parafoil motion to the vehicle. Parafoil deployment brakes refer to the deflection of the trailing edge used to limit the magnitude of the surge associated with the transition of the system from ballistic to forward flight. These deployment brakes are released (initiated by predetermined pencil cutters) following confluence separation.

The parafoil has a preset differential control surface setting that, following the pencil cutter initiated release of the parafoil deployment brakes, places the vehicle into a slow turn. The navigation guidance and control system (NGCS) releases the built in turn and begins to fly the vehicle autonomously following brake release. Should the NGCS fail to function, the footprint of the test article would be limited to a predetermined radius that would drift with the prevailing winds. The NGCS, built by Steve Snyder Enterprises, consists of an onboard computer system with software that uses global positioning system (GPS) data, a barometric altimeter, and a compass to control autonomously and steer the test article to a predetermined target. With the aide of a laser altimeter, the NGCS is programmed to perform a flared landing. The parafoil is steered like a square personnel parachute, using winches to deflect the outer 25% of the trailing edge to effect turns and alter the lift to drag ratio L/D of the parafoil system. The NGCS is equipped with a receiver that allows a ground station to transmit real-time user input parafoil control surface commands, referred to as manual mode. Manual mode has been used to perform an extensive series of parafoil maneuvers to extract the aerodynamic characteristics of the system.[3,4] This process and the results will be discussed in further detail later in this paper. These maneuvers have included flap settings, flares at altitude, and turns using various combinations of differential control surface settings.

Description of Low-Velocity Air Drop Test Articles

Before being tested on a lifting body configuration, development testing of the primary and backup parachute system was conducted by the X-38 project at the U.S. Army Yuma Proving Ground (YPG), Arizona. These low-velocity air drop tests, referred to as phase 2, were performed using a C-130 aircraft and a standard cargo platform with a weight tub attached and the parachute system rigged to the top of the weight tub (Fig. 1). The platforms ranged in size from 16 to 24 ft (4.9 to 7.3 m) in length and in weight from 7000 to 22,000 lb (3174 to 9979 kg). The test articles were extracted from

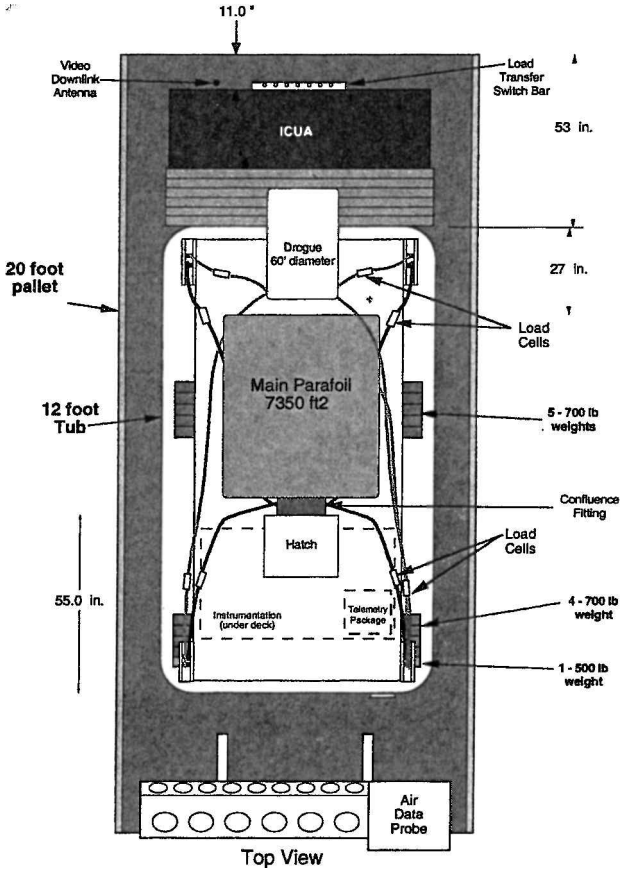

Fig. 1 Typical pallet test article.

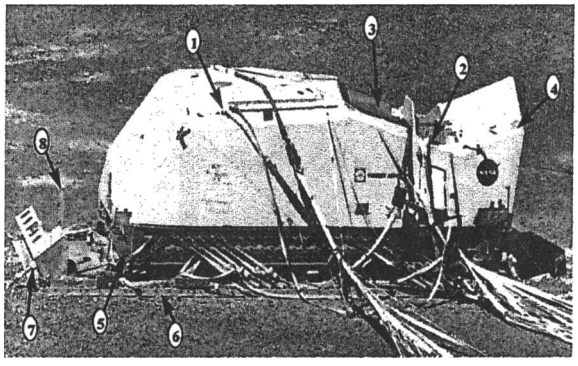

Fig. 2 Doghouse test article: 1) drogue and parafoil forward four-point attach fitting, 2) drogue and parafoil aft four-point attach fitting, 3) parafoil compartment, 4) drogue two-point attach fitting, 5) standard weight tub (Doghouse actually welded to tub), 6) standard C-130 cargo pallet, 7) deployable ADP housing, and 8) compass for NGCS.

the C-130 aircraft at altitudes ranging from 7000 to 18,000 ft (2134 to 5486 m) msl at 130 kn (67 m/s) indicated airspeed.

As the development testing at YPG proceeded, a 20-ft (6.1 m) long weight tub (named the Doghouse) was modified to simulate the various parachute compartments and attach fittings on V-131 (Fig. 2). Careful attention was taken to simulate accurately various aspects of V-131 that would affect the parachute system including the main drogue compartment, the main drogue initial two-point attach fittings, the channels used to route the drogue attach slings from the two-point to four-point attach fittings, the main parafoil compartment, the channels used to route the parafoil forward attach slings to the parafoil compartment, the backup system compartment, and the primary and backup mortars. This geometric modeling included the relative locations of all of the compartments with respect to each other and with respect to the attach fittings.

Each test article was equipped with a primary and backup sequencer, each one completely independent of the other, and either capable of releasing the drogue and deploying the parafoil. In the case of the Doghouse, the sequencers were capable of releasing the stabilization parachute, initiating the mortar, repositioning the primary drogue, releasing the primary drogue, releasing the main parafoil, initiating the backup mortar, and releasing the backup drogue (which would deploy the backup main).

The phase 2 test articles were equipped with a suite of instrumentation that changed as the program matured. At present, the instrumentation system is an entirely onboard data system using GMH Engineering Data Bricks with low-pass filters, sampling at 50 Hz to record as many as 27 parameters ranging from deployable air data probe (alpha, beta, static, and total pressure several feet ahead of and below the leading edge of the pallet), motion pack (triaxial accelerometer and rate gyro package mounted inside the weight tub), parafoil control winches (supply voltage, motor current, and control line position and load), pallet inclinometer, and two discrete signals such as pallet first motion and bag motion. Additionally an impact recorder was hard mounted to the weight tub. This self-contained triaxial accelerometer package and data system that records discrete events triggered when any accelerometer senses an acceleration that exceeds a user-programmed threshold is built by Instrumented Sensor Technology. The touchdown acceleration profile has been used in a mathematical model that estimates the physiological effect of landing loads on the human body [referred to as Brinkley analysis (see Ref. 6)]. Both a 16-mm high-speed film camera and a downlinked video camera were mounted on each test article with an upward field of view to capture the deployment and inflation of the parafoil.

To better understand the total and chordwise load distribution associated with the parafoil deployment and full flight, a new type of stand alone instrumentation was developed by NASA Johnson Space Center and Invocon Inc.[7] The riser tension measuring system units were programmed and clamped onto the dispersion risers before the parafoil being packed. The units were armed as the risers were extracted from the deployment bag, recording both opening loads and full-flight steady-state loads.[8] The riser tension measuring system units have also been used to measure the deployment line loads during both drogue and parafoil deployment. With the initial success of the tension measuring system units on the risers (in particular their ability to survive packing and deployment), they were modified and implemented to measure the loads in the parafoil lower surface leading-edge reinforcement tape to assist in resolving anomalies. A third application of tension measuring system-type data system being tested is the parafoil inclinometer system. Through measuring the output of a series of single- and multiaxis accelerometers sewn to the interior floor of the center cell of the canopy during flight and combining these data with trajectory information, the X-38 parachute group is attempting to measure the steady-state trim angle of attack of the parafoil.

Primary Recovery System Testing Overview

This section will discuss the primary accomplishments of the X-38 parachute testing to date. The first four tests of the primary parafoil system were of limited success. Of the tests where the parafoil was deployed, all three suffered from very soft parafoil inflation and stage disreefing. A series of tow and drop tests of a subscale 750-ft^2 (69.7 m^2) model canopy, almost identical in design to that of the full-scale canopies, was conducted at YPG to assess the parafoil system (Fig. 3). The payload mass used for the subscale tests was calculated using mass ratio scaling. Iacomini and Madsen discuss the subscale tests, in particular the rigging angle studies, in detail.[9]

Several significant shortcomings of the full-scale system were identified. The upper surface fabric had high porosity (values ranging from 25 to 28 ft^3/min (0.71 to 0.79 m^3/min) were measured on the canopies tested), which tended to aggravate other shortcomings of the design. In particular, the high porosity fabric tended to cause slow pressurization of new cells during disreef and make the leading edge more prone to flow separation. The line length ratio was large ($R/b = 1.0$), which, although impervious to small canopy

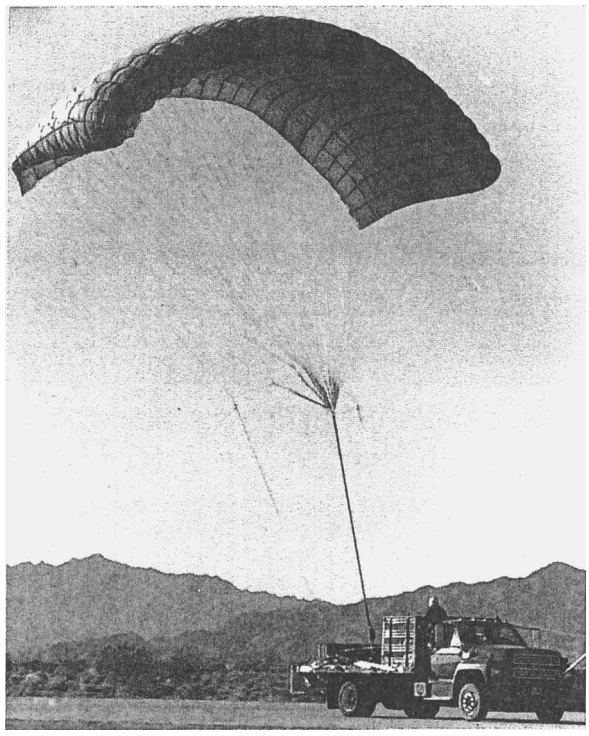

Fig. 3 Tow testing 750-ft^2 parafoil.

to payload perturbations, would not damp out large perturbations such as the system was experiencing. The aspect ratio was large, such that during parafoil disreef the canopy was experiencing very pronounced deformations. The rigging angle for the airfoil shape and inlet being implemented was too shallow. This resulted in the canopy trimming at an angle of attack close enough to stall (aided by the porous upper surface) that perturbations such as brake release could result in the canopy stalling and or collapsing.

Two 3600-ft^2 (334.5 m^2) canopies were prepared with all of the improvements identified in subscale testing. The fifth and sixth drop tests were a direct comparison of two 3600-ft^2 (334.5 m^2) canopies. The fixes implemented on drop 6 included decreasing the aspect ratio AR of the parafoil from 3.0 to 2.7, increasing the rigging angle from 10 to 13 deg, reducing the line length ratio R/b from 1.0 to 0.6, and reducing the porosity of the canopy. The fabric porosity was reduced by applying a B.F. Goodrich urethane to the upper and lower surface of all cells, from the leading edge aft to the 40% chord station. All of the fixes implemented on drop 6 were flown on drop 5, except the line length ratio, which was kept at the original 1.0 value. Neither test article was equipped with an NGCS or winches. The parafoil deployment for drop 5 was typical of the first few tests with large vehicle oscillations with respect to the parafoil that did not fully damp until after releasing the deployment brakes. Drop 6 was a major improvement with dynamics associated with the deployment and disreefing damping quickly. Other improvements suggested by the industry experts brought on the parachute test and development team during the subscale testing could not be reasonably implemented without constructing a completely new canopy; construction of a new 5500-ft^2 (511.0 m^2) canopy was begun.

The new parafoil design (referred to as generation 2) was a 5500-ft^2 (511.0 m^2) canopy with zero porosity fabric on both the upper and lower surface, with shaped panels used in the construction of all surfaces and implemented construction techniques to minimize deformation of the airfoil shape (among many other minor changes). The fundamental airfoil shape used in the parafoil was not changed; therefore, the limitations associated with the inlet shape and stagnation point could not be eliminated. The first flight of the new generation 2 design on drop 13 was very successful. Again manual initiated maneuvers were executed to begin to build an aerodynamic database for the new generation 2 design for use in simulation programs.[3,4]

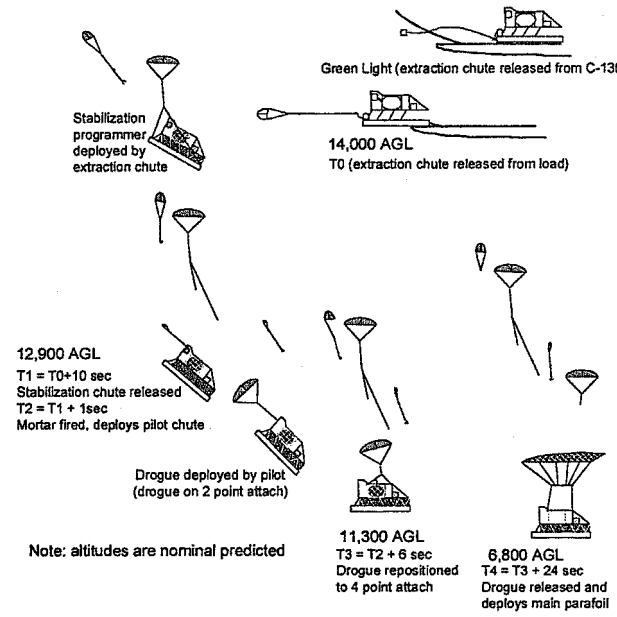

Fig. 4 Doghouse test sequence (P2D16).

Drop 16 was the second flight of the Doghouse, this time deploying a 5500-ft^2 (511.0 m^2) parafoil canopy (Fig. 4). The Doghouse was extracted using an extraction parachute, which in turn deployed a drogue parachute that stabilized the Doghouse. The sequencer then released the stabilization parachute and fired the main system mortar. The mortar deployed the pilot parachute, which in turn extracted and deployed the drogue. From this point the drogue was repositioned to directly above the Doghouse and subsequently released deploying the parafoil. The parafoil was successfully deployed and, unlike earlier flights, the guidance system was allowed to fly autonomous to touchdown. A failure of the barometric altimeter prevented the autosystem from accepting laser altimeter data and performing a flare at touchdown. However, the NGCS did steer the Doghouse into the wind at landing.

Although the parafoil deployments with the generation 2 parafoil were significantly improved over those of the generation 1 parafoil, the initial dynamics were still unpredictable with the parafoil and payload getting into coning dynamics that would not damp out until well into the third stage of the parafoil deployment. The nine-cell first-stage parafoil has a large line length ratio, $R/b = 2.14$, a low aspect ratio, $AR = 0.78$, and a low arc anhedral, ~6.7 deg, all of these factors contributing to the inherent instability in the first stage. Again, after running several series of subscale drop tests using a 750-ft^2 (69.7 m^2) canopy, the project decided to pursue a more benign initial opening by implementing a Rueter wrap around the suspension lines. This approach effectively attempts to make the rectangular first-stage planform act more like a round parachute. This initial parafoil deployment stage became know as zero reefing (Fig. 5).

For drop 19, the zero reefing line was strengthened, and it held for the planned first 4 s of deployment. When the zero reefing line was cut, the parafoil flattened out into first stage, and the floor of the first stage failed at the leading edge of the center cell. The resulting failure raced back to the trailing edge and split the canopy in half. The test article spiraled to the ground under half a canopy (the other half had collapsed) and was a loss. Once again, several weeks of subscale testing using a 750-ft^2 (69.7 m^2) parafoil were performed. The results of the tests (using primarily riser and leading-edge tension measuring system units) showed that on releasing the Rueter wrap the lower surface experiences a momentary large load spike associated with the change in geometry of the parafoil. Improvements were made by strengthening of the lower surface first-stage material and adding leading-edge reinforcement to improve how the lower surface leading-edge load is transferred across reefed stages.

Drop 20 was another attempt at zero reefing deployment of the parafoil. The zero reefing line held through deployment, and when

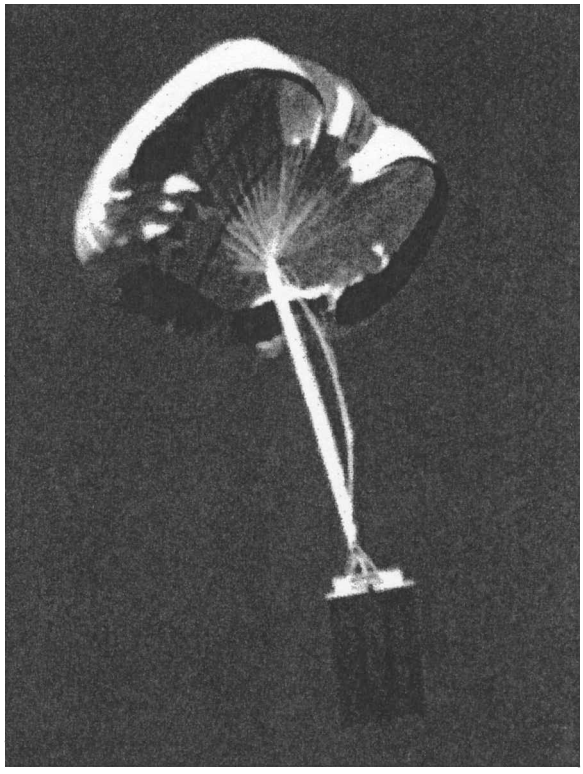

Fig. 5 Zero reefing full-scale test (before releasing zero reefing line P2D20).

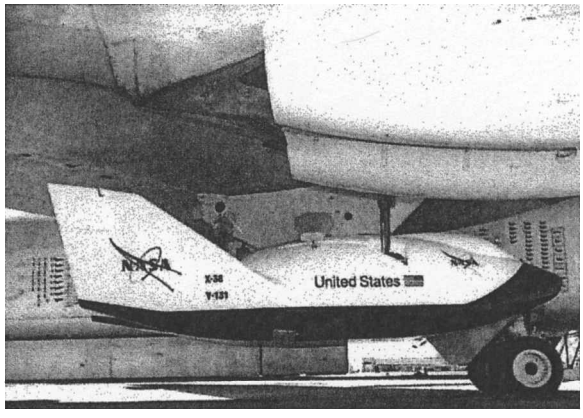

Fig. 6 V-131 mated to the B-52.

cut, the canopy successfully transitioned from zero to first stage. The ensuing deployment was uneventful with the dynamics being fairly benign, but again the confluence fitting failed to separate when the restraining cut loop was severed. Posttest modifications where made to the confluence to increase the clearance of the two halves and the restraining sheer pins.

The next test of the parafoil system, phase 3 drop 1, was conducted using V-131 at NASA Dryden Flight Research Center. This was the first test using a parafoil to land a lifting body released from the wing of the NASA B-52. V-131 is 24 ft (7.3 m) in length and weighed 15,000 lb (6804 kg) fully equipped (Figs. 6–8).

V-131 had a flight computer that could deploy the primary parachute system and activate the NGCS to steer the vehicle just as in the phase 2 tests at YPG. If commanded to, the flight computer could release the primary system and deploy the backup parachute system. The first flight of V-131 was conducted using the 5500-ft^2 (511 m^2) generation 2 parafoil with zero reefing. The vehicle was released from the wing of the B-52 at 23,000-ft (7010 m) msl. Deployment of the primary parachute system was initiated 5 s after release. The pilot parachute extraction of the drogue and the drogue reposition took place just as demonstrated during the Doghouse

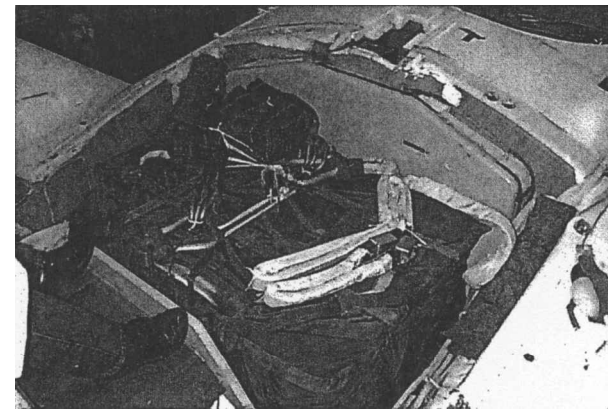

Fig. 7 Parafoil rigged to V-131.

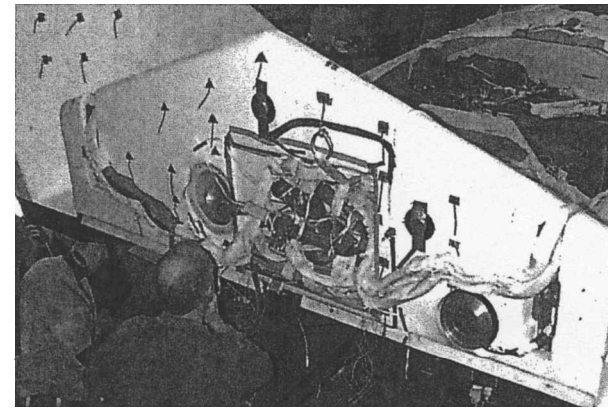

Fig. 8 Primary drogue rigged to V-131.

tests. The drogue sustained substantial flutter damage to the gores that were not part of the pressurized portion of the canopy during first stage; however, the damage did not affect the overall performance of the drogue. The main was deployed by the drogue and inflated in zero stage, but the roof panel of cell 17 (part of fourth stage) was damaged. The roof panel had sustained burn damage during extraction from the deployment bag and failed during initial pressurization. Whereas the floor of the stages subsequent to first stage are held reefed by a system of reefing lines and so do not experience first-stage dynamic pressure, the inlets are not reefed closed. This allows subsequent stages to attempt to inflate despite that they can not spread due to the reefing lines along the floor. The roof of cell 17 was split from nose to tail. When the zero reefing released, the canopy surged backward and continued to fly backward until disreef to second stage at which point the canopy transitioned to forward flight through a partial collapse of the leading edge. The canopy recovered in forward flight and disreefed through third, fourth, and fifth stages without further incident, and the confluence separated as planned. The vehicle was flown in manual mode all of the way to touchdown with the failure of the roof panel on cell 17 appearing to have very little if any effect on the performance of the parafoil (Figs. 9 and 10).

Once again, after several months of subscale testing with a 750-ft^2 (69.7 m^2) canopy, the parachute group produced a new technique to eliminate the randomness that the rebound following parafoil line stretch was creating. Subscale testing indicated that attaching an energy modulator between the drogue and the upper surface of the center of the parafoil created a repeatable presentation of the canopy to the airstream (the modulator when fully stroked released the parafoil).[10] Along with promoting the spanwise spreading of the first-stage canopy, this energy modulator would give other techniques involving the packing of the nose and tail a predictable and repeatable starting point for presentation to the airstream (Fig. 11). As the subscale testing progressed, the surge associated with the first stage transitioning from flat plate ballistic flight to forward

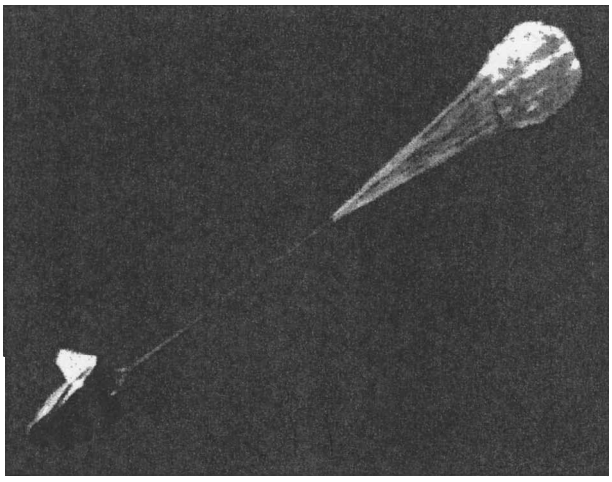

Fig. 9 Phase 3 drop 1 drogue on two-point attach.

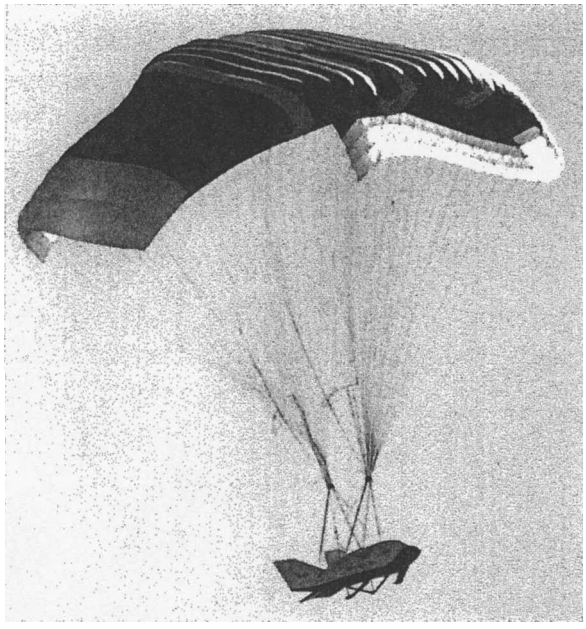

Fig. 10 Phase 3 drop 1 parafoil in full flight (flaps deflected) with vehicle landing gear deployed.

flight was determined to be too large. The surge would set the payload and parafoil into a two-body motion that would not damp out until well into parafoil second or third stage. Through subscale testing it was established that the shallower rigging angles tended to always transition from flat plate to forward flight with less surge, but also tended to be less stable in roll. The steeper rigging angles were more prone to flying backward momentarily before transitioning to forward flight (and with a more vigorous surge) than the shallower rigging angles, yet were more stable in roll. The 10-deg configuration was the preferred rigging angle, a compromise between first-stage surge, roll stability, and not trimming too close to stall angle of attack. Along with investigating the effects of rigging angle on opening dynamics, deployment brake settings for the various rigging angles where also investigated.[9] Work is continuing on determining how the subscale rigging angle scales up to full scale.

Increasing the aspect ratio of the first stage by adding two cells for a total of 11 cells ($R/b = 1.74$, $AR = 0.95$, and arc anhedral $\approx$8.2 deg) was also investigated. This was prompted by the observation that the nine-cell first-stage canopy held from deployment all of the way to touchdown did not appear to have strong damping to the dynamics associated with first-stage inflation and transition from flat plate to forward flight. The second stage parafoil, with a total of 15 cells, $R/b = 1.3$, and $AR = 1.3$, was observed to eventually always

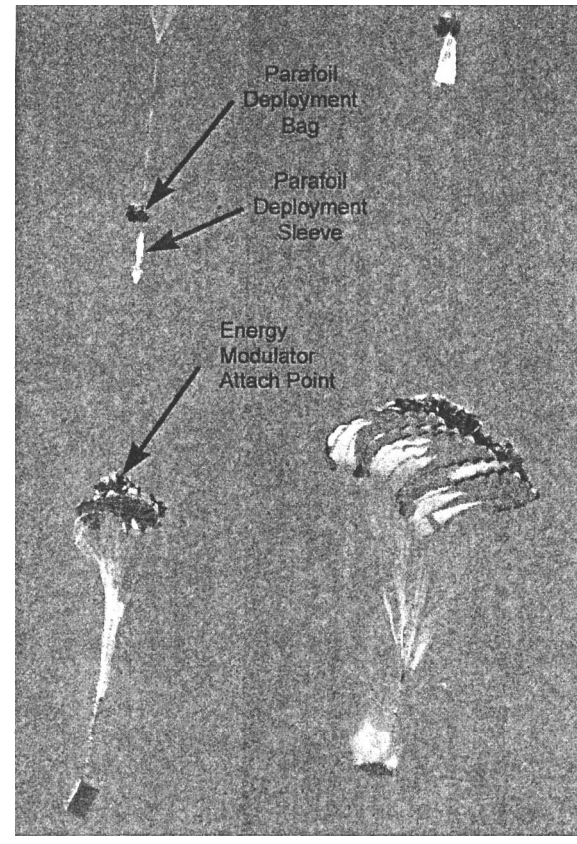

Fig. 11 Subscale deployment implementing parafoil upper surface energy modulator.

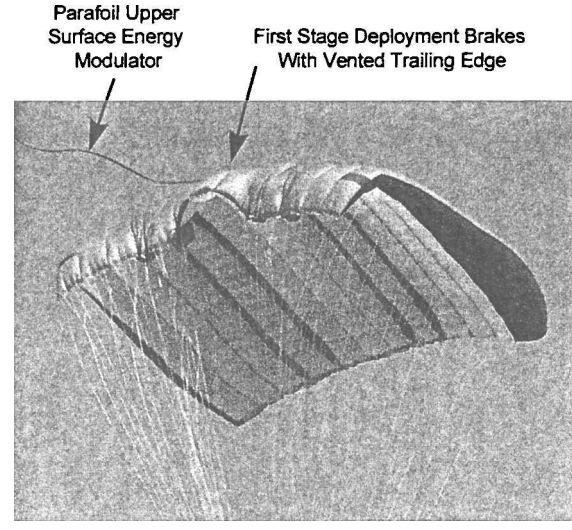

Fig. 12 Subscale 11 cell first-stage parafoil.

damp out any parafoil to payload oscillations. Another parameter investigated was venting the trailing edge of the deployment brakes by allowing the center three cells of the first stage to fly free. This was achieved by not pulling the entire trailing edge down as part of the deployment brakes (Fig. 12). This change was found to improve directional stability of the canopy during transition to forward flight. The potential improvements investigated in subscale testing were baselined for full-scale testing on drops 22 and 23.

Because moving back to 10-deg rigging angle was not a change that was approached without caution, drop 22 had a rigging angle of 13 deg and drop 23 had a rigging angle of 10 deg. Both drops implemented all of the other changes discussed from the subscale testing. Both drops had greatly improved openings over any prior test. Drop 22 had a very symmetric first-stage spreading and a surge that, while

Table 1 Summary of X-38 full-scale tests

Test	Date	Parafoil area, ft^2	Touchdown Hdot, ft/s	Touchdown Impact vertical, g	Crewmember injury risk ill or injured	Parafoil canopy deployment Overall assessment	Parafoil canopy deployment Damage
P2D1	Aug. 95	3600				Poor	Minor burns
P2D2	Sept. 95	7350				Poor	Minor burns
P2D3	Dec. 95				See/Note[c]		
P2D4[a]	April 96	7350	23	27	High	Very poor	Minor
P2D5A	Oct. 96	3600				Poor	Minor
P2D6	Oct. 96	3600	26	51	>High	Average	Minor
P2D7	Dec. 96	3600				Poor	Minor
P2D9	Feb. 97	3600				Poor	Many burns
P2D8A	Feb. 97	7350	25	40	>High	Average	Minor
P2D11	March 97	7350	24	31	>High	Average	Minor
P2D13[a]	May 97	5468	21	18	High	Average	Minor
P2D14	May 97	7350	27	41	>High	Average	Minor
P2D15	July 97	5468	21	21	>High	Average	Minor
P2D16	July 97	5468	n/a	47	>High	Average	Minor burns
P2D17	Sept. 97	5468	22	51	>High	Average	Minor burns TE
P2D19	Oct. 97	Parafoil failed immediately following release of zero stage reefing					
P2D20	Dec. 97	5468	25	46	>High	Average/good	Minor burns TE
P3D1	March 98	5468	17	9	Low	Poor	Several cells
P2D21	June 98	5468	21	32	High	Poor	Stabilizer torn
P2D22[b]	Oct. 98	5468	14	11	Low	Good	Minor/none
P2D23	Oct. 98	5468	23	25	Moderate	Good	Minor/none
P2D24[b]	Nov. 98	5468	15	11	Low	Good	Minor/none
P2D25	Dec. 98	5468	17	16	Low	Very good	Minor/none
P2D26	Dec. 98	5468	15	13	Low	Very good	Several cells
P3D2[b]	Feb. 99	5468	18	6	Low	Very good	None
P3D3[b]	March 99	5468	10	12	Low	Very good	None

[a]Partial flare. [b]Flare landing. [c]On P3D3, in an attempt to release the test article from the pallet, the drogue was cut away without deploying the parafoil.

pronounced, stayed in the longitudinal plane and damped out almost immediately. The remainder of drop 22 was very successful, with several maneuvers and landing with an autoflare resulting in a rate of descent of 14 ft/s (4.3 m/s) at touchdown.

Drop 23 had less of a surge, but for reasons not yet fully understood, the canopy did not stay directly above the pallet during the initial first-stage flat plate spreading. By the time the canopy began to surge to forward flight, it was far enough off the vehicle heading vector (wind line) that the surge became a coning motion. Although it did damp before disreef to third stage, the coning motion also swung the payload around in a fashion that was considered unacceptable. Subsequent disreefs took place without incident. When the NGCS went to release the range safety built in turn, a short in the winch command circuit drove one winch to 100% control stroke. This resulted in stalling that side of the wing. When manual control became available to the ground team, the system was in a steep spiral dive. Eventually the stable flight was recovered by a combination of trailing-edge control line crows feet failing, commanding the opposite winch to a deep control stroke setting, and the stalled portion of the canopy reinflating. The test article was landed safely, and no maneuvers or autoflight were performed.

The program chose to keep the configuration flown on drop 22 (13-deg rigging angle) and repeat the test before flying a lifting body again. On drop 24 during the first-stage transition from flat plate flight, the canopy flew backward momentarily before establishing forward flight and inflating the first-stage cells of the wing. Second-stage disreef was very soft with the tip of the parafoil remaining soft throughout most of the third stage. Disreef to fourth stage with a soft second stage could have resulted in the loss of an entire half of the canopy. The canopy established a fully rigid wing late in the third stage and disreefed to fourth and fifth stages without incident. The remainder of the flight went well, landing with another autoflare and achieving a rate of descent 15 ft/s (4.6 m/s) at touchdown. Rather than risk having a partial collapse of the canopy late in the disreefing sequence, the program decided to run two more tests at YPG using pallets only; this time the rigging angle was decreased to 10 deg. The following two pallet tests, P2D25 and P2D26, both had highly successful parafoil deployments, and the program has kept the rigging angle of 10 deg for all subsequent full-scale tests.

The most recent tests conducted were the second free flight of V-131 (phase 3 drop 2), and the first free flight of V-132 (phase 3 drop 3). For phase 3 drop 2, the vehicle was in free flight for 4 s before the recovery system was initiated. For phase 3 drop 3, the vehicle was in free flight for 12 s. For both tests, positioning the drogue 15 ft (4.6 m) farther aft of the vehicle to avoid sustaining flutter damage proved successful. For both tests, the parafoil deployment was very successful with no damage noted on the main parafoil on either test. Three maneuvers were conducted on both tests followed by autoflight with the NGCS performing an autoflare at landing. On P3D2 the flare was triggered early due to loss of the laser altimeter (frost/condensation had formed on the laser window), which resulted in a rate of descent of 18 ft/s (5.5 m/s) at touchdown. However on P3D3, the flare was almost perfect with a rate of descent at landing of $10\frac{1}{2}$ ft/s (3.2 m/s). Table 1 summarizes the X-38 full-scale parachute tests that have been conducted at either YPG or NASA Dryden Flight Research Center to date.

Aerodynamic Database and Flight Data Sources

Initially, the X-38 parafoil performance team reviewed several aerodynamic data sources including that developed by The Boeing Company for Pioneer Aerospace Corporation under contract to NASA Marshall Space Flight Center in the advanced recovery systems (ARS) study. Additional critical sources were parafoil wind-tunnel test results obtained from the ARS2 program,[11] NASA Langley Research Center,[12] and Nicolaides.[13] Early subscale parafoil tow tests enabled further early modifications to the aerodynamics database, as well as estimates of correlated angles of attack. This original database created through the compilation of sources laid the groundwork for trends as a function of angle of attack. The C_L, C_D, and $Cm_{c/4}$ vs angle-of-attack slopes have all been preserved thus far. Recent modifications to the aerodynamic database came from the analysis of full-scale drop test data as a function of flap setting and are presented here along with an initial estimate of associated angles of attack necessary to utilize the database correctly. The analysis of the parafoil longitudinal characteristics has been performed while the parafoil system is in trimmed, steady-state flight as diagrammed in Fig. 13. For a given rigging angle and

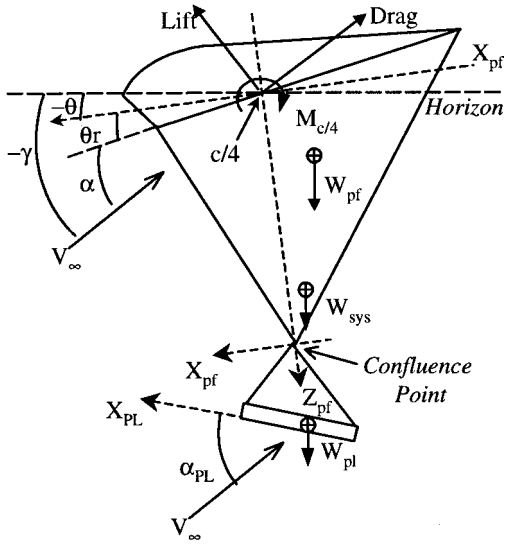

Fig. 13 Parafoil system in equilibrium glide.

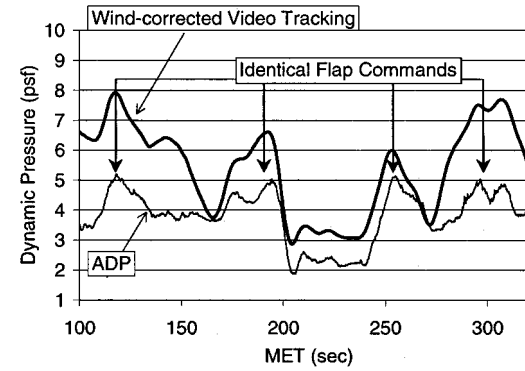

Fig. 14 Example comparison of different dynamic pressure sources (P2D25).

flap setting, the parafoil equilibrium state should result in a constant dynamic pressure and flight-path angle.

During the development of the aerodynamic database for the parafoil dynamic simulation (PDS) being developed at NASA Johnson Space Center,[3,4] a number of maneuvers were performed during the phase 2 tests. These maneuvers were performed by up linking to the NGCS commands that were designed to achieve steady-state flight conditions such that the onboard instrumentation combined with test article trajectory information could be used to compare with the predicted performance using PDS. Several data sources were used to extract longitudinal aerodynamic coefficients. Velocity measurements in the X (east), Y (north), and Z (up) components were taken to compute flight-path angle and, combined with measurements of density, to compute dynamic pressure. As available, dynamic pressure was also measured directly from an air data probe or flush air data system. Wind direction and magnitude vs altitude were used to correct the velocity data for effects induced by winds. Control line position data was recorded to confirm exactly what flap inputs were given to the parafoil. Data used to extract turn rate trends include vehicle yaw rate data; velocity measurements in the X (east) and Y (north) components to compute heading and heading rate; wind measurements, direction, and magnitude to correct the velocity data for effects induced by winds; and control line position data to confirm exactly what turn inputs were given to the parafoil.

For the phase 2 drops, velocity data were collected by video tracking data with an estimated accuracy of ± 1 ft/s (± 0.30 m/s). For the phase 3 drops, the velocity data were collected by the onboard embedded GPS/inertial navigation sensor (INS) (EGI) system with a stated accuracy of ± 0.5 ft/s (± 0.15 m/s) in X and Y and ± 1.0 ft/s (± 0.30 m/s) in Z. Three wind data sources were available for applying wind corrections to the velocity data. Balloons were typically launched hourly, with the dataset closest to the actual test article release considered the best source for winds from balloons. Balloons also provided the only source of atmospheric conditions such as density and temperature vs altitude. Another wind data source is the parafoil onboard NGCS estimated wind. The NGCS estimate, based on expected performance and GPS trajectory, is better in straight flight when the parafoil is not turning. Though some flights experienced many turns, the NGCS estimated winds occasionally appeared more reasonable than the balloon measurements. Therefore, a combination of balloon and NGCS estimated wind data was sometimes used.

System performance is best judged with data seen by the system. For this reason, it is important to ensure the velocity data used in performance calculations are the velocities seen by the parafoil relative to the air mass. The wind corrected velocity V_{wc} for the payload was calculated using the velocity components V_x and V_y, wind data, and the following equations:

$$V_{x_{wc}} = V_x - V_w \sin(\phi w - 180) \tag{1}$$

$$V_{y_{wc}} = V_y - V_w \cos(\phi w - 180) \tag{2}$$

$$V_{wc} = \sqrt{V_{x_{wc}}^2 + V_{y_{wc}}^2 + V_z^2} \tag{3}$$

Balloon and NGCS data do not provide vertical wind information. Therefore, the vertical velocity is not wind corrected. However, because vertical wind components are believed on average to be very small compared to the horizontal component of wind, neglecting the vertical wind is considered a fair assumption. Calculating longitudinal aerodynamics is heavily dependent on knowledge of dynamic pressure. The source of dynamic pressure has been an issue throughout the X-38 parafoil development program. One source of dynamic pressure relies on postflight calculations based on ground relative tracking data and wind data collected via balloons launched before or after the drop test:

$$\bar{q} = \tfrac{1}{2}\rho V_{wc}^2 \tag{4}$$

Because balloon data are not collected exactly along the path the vehicle actually travels through the air, there is always some error present in the wind data and, thus, in the calculated wind-corrected dynamic pressure. Another method of obtaining dynamic pressure is directly through the air data probe (ADP) or flush air data system (FADS). In Fig. 14, for a given flap setting, the ADP consistently measures approximately 5 psf (239 pa) where the wind-corrected video tracking data measures as high as 8 to as low as 6 psf (383 to 287 pa). Differences between the two sources are credited to errors in the balloon wind measurements.

The flaps are defined as the outer quarter span of the canopy with only the trailing-edge line group being pulled down. Positive deflection or stroke is a downward movement of the flaps due to retracting the control line using the winches. Control line position or deflection (CLD) data are noted in either inches or percentage of stall stroke (%SS). Stall stroke is defined as the amount of CLD necessary to induce the onset of parafoil stall or collapse. The control stroke required to induce parafoil collapse[9] is a function of the parafoil rigging angle. Throughout the X-38 parafoil development program, the project investigated a range of rigging angles (RA) from 4 to 16 deg, with most of the testing focused on 10 and 13 deg. The estimate for 100% of stall stroke for the 5468-ft^2 (508 m^2) parafoil is $\approx$227 in. (5.8 m) for RA of 10 deg and $\approx$314 in. (8.0 m) for RA of 13 deg. In this work, differential commands, or turn commands, are listed with the left control line position first, followed by the right. For example, a 13-deg rigged 5468-ft^2 (508 m^2) parafoil performing a left turn with a base, or minimum, stroke of 0 in. and a differential deflection of 157 in. (4.0 m) would be listed as L0/R50 %SS.

Parafoil Performance Calculations

This study calculates the overall system coefficients of lift, C_L and drag, C_D, rather than strictly parafoil C_L and C_D. This is done because the separate effects of the payload, suspension lines, etc., are difficult to identify and separate from the collected flight-test

data. However, from simulation tests, it has been determined that the payload drag and lift are small compared to the overall system characteristics and do not vary results significantly. Once again, note that in calculating C_L and C_D this study only analyzes flight-test data of steady-state conditions. The equations derived to obtain C_L and C_D assume all external forces acting on the system are in equilibrium and the system is, thus, in equilibrium glide. Additionally, steady-state turn data are not used in the analysis. The longitudinal aerodynamic database for the 5468-ft^2 (508 m^2) parafoil is currently based on approximately symmetric control surface deflection maneuvers, or flaps. Although equal flaps are commanded, ensuring that both control lines deflect the exact same amount is difficult. Therefore, in analyzing the flight data, any command with a differential deflection that was less than 4%SS was assumed suitable for this study. For example, 50%SS flaps implies that both the left and right control lines are deflected an average of 50%SS with a differential deflection of less than 4%SS. Given these assumptions, calculating the C_L and C_D for the system is rather straightforward. Starting from aerodynamic textbook definitions,[14]

$$\text{lift} = \bar{q} C_L S \tag{5}$$

$$\text{drag} = \bar{q} C_D S \tag{6}$$

$$\gamma = a\tan(V_z / Vh_{\text{wc}}) \tag{7}$$

Note that the flight-path angle is negative for a parafoil because V_z will be negative. For steady-state flight, Fig. 13 shows

$$\text{lift} = W_{\text{sys}} \cos(\gamma) \tag{8}$$

$$\text{drag} = -W_{\text{sys}} \sin(\gamma) \tag{9}$$

Note the system weight in an equilibrium glide state includes the weight of the payload and entire parafoil system but excludes the parafoil's enclosed air and apparent mass. Thus, combining Eqs. (5–9), C_L and C_D for equilibrium flight can be written as

$$C_L = \frac{W_{\text{sys}} \cos(\gamma)}{\bar{q} S} \tag{10}$$

$$C_D = \frac{W_{\text{sys}} \sin(\gamma)}{\bar{q} S} \tag{11}$$

Steady-state maneuvers within each drop test were analyzed. Being independent of altitude, C_L and C_D should achieve constant values. In analyzing each maneuver, an average over the maneuver time is not begun until initial dynamic response has settled (Fig. 15). The averaging time ends before the next maneuver is commanded. Experience has demonstrated that typical response time to flap deflection input is on the order of 15 s. The response time of course fluctuates proportionally to the maneuver size, after which, the system achieves a state resembling equilibrium glide.

Usually dynamic pressure and flight-path angles are calculated using trajectory data corrected for winds with balloon data. However as already stated, to minimize the effects of wind errors, it is

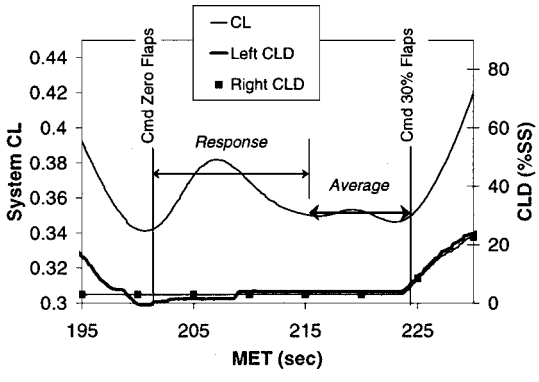

Fig. 15 Typical response to flap deflection input (P2D13).

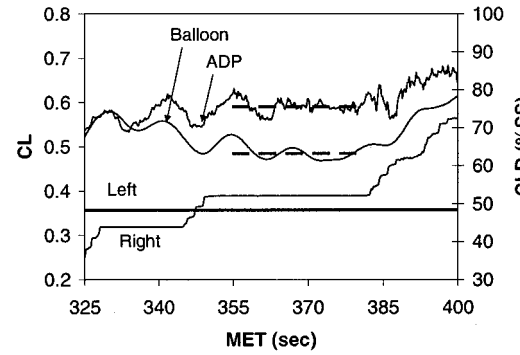

Fig. 16 Wind error effect on C_L calculation (P2D15).

preferred to use dynamic pressure directly from the ADP or FADS if available. The dynamic pressure measurement can also be used to yield a better wind-corrected flight-path angle. First, atmospheric density from the balloon data is used to back out the wind-corrected total velocity from the ADP (or FADS) dynamic pressure solving for V_{wc} in Eq. (4). Again, neglecting any vertical winds, the tracking data V_z can be used in place of Vh_{wc} in Eq. (7) to calculate flight-path angle. This flight path is then used in Eqs. (10) and (11) with the ADP (or FADS) dynamic pressure rather than values derived from the wind-corrected tracking data. In this method, errors in C_L and C_D calculations due to wind uncertainties are usually reduced because the wind information is taken from the vehicle's path through the atmosphere and not from another location and time. The benefits of using a direct dynamic pressure source for C_L and C_D calculations are exemplified in Fig. 16. At the beginning of Fig. 16, one can see that C_L calculations align for either dynamic pressure source. By mission elapsed time (MET) 340, the balloon derived C_L decreases compared to that derived using the ADP, and the variation in C_L over the time average 355–380 s is larger in the balloon-derived data.

With the existence of equilibrium glide, the moments about the confluence fitting should equal zero. When Fig. 13 is referred to, and normalizing by dynamic pressure times area,

$$Cm_{\text{Conf}} = Cm_{c/4} + (Z_{c/4}/c)[C_L \sin(\alpha + \theta_r) - C_D \cos(\alpha + \theta_r)] - (W_{\text{pf}}/\bar{q}S)[(X_{\text{cg}}/c)\cos(\theta) + (Z_{\text{cg}}/c)\sin(\theta)] \tag{12}$$

$$\theta = \alpha + \theta_r + \gamma \tag{13}$$

Also for equilibrium flight from Eqs. (10) and (11),

$$\bar{q} = W_{\text{sys}} \Big/ S\sqrt{C_L^2 + C_D^2} \tag{14}$$

$$\gamma = -a\tan(C_D / C_L) \tag{15}$$

Note again that the simplifying assumption is C_L and C_D are derived for the total parafoil system and payload, instead of taking into account the separate contributions of the canopy, lines, etc., as does Lingard.[15] The C_L and C_D are then used to calculate the system moment coefficient about the quarter chord point, $Cm_{c/4}$, as if they are parafoil properties only. To solve for $Cm_{c/4}$, either angle of attack or pitch angle of the parafoil must be known. However, measuring either of these quantities on a large-scale parafoil is extremely difficult and until only recently had not been done. Unlike instrumentation used on rigid the structure of airplanes, any parafoil instrumentation has to be small and robust enough to withstand the forces of pressure packing followed by rapid deployment and inflation loads. The results of three separate techniques suggest that the parafoil rigged at 13 deg trims at an angle of attack of approximately 4 deg. The technique presented by Martin,[8] using the in flight measurement of the chordwise lift distribution, supports Lingard's[16] assertion that trim angle of attack does not change as a function of flap setting.

Yaw rate data were collected via either an EGI system with an estimated accuracy within ±0.04 deg/s or a self-contained gyro package with an estimated resolution of 0.025 deg/s. However, caution

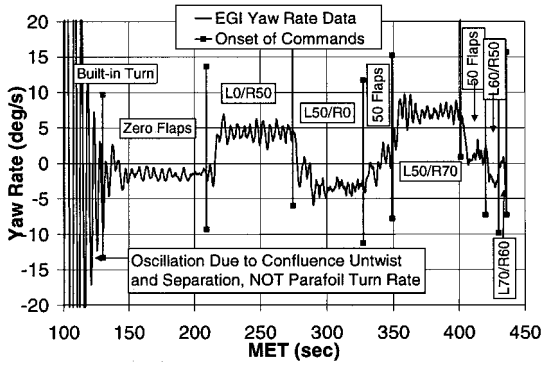

Fig. 17 Yaw rate data example (P3D1).

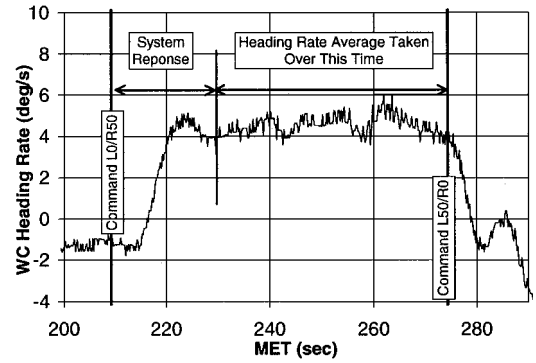

Fig. 18 Typical example of parafoil system response to turn input (P3D1).

should be exercised when using payload body yaw rate data. The data are typically more indicative of vehicle motion and not necessarily that of the parafoil. Parafoil turn performance can not be determined with much confidence via yaw rate data if the confluence fitting does not separate because this causes the vehicle to have very lightly damped yaw coupling to the parafoil. As a result, the vehicle continually oscillates underneath the parafoil (Fig. 17). With a properly separated confluence fitting, the vehicle motion is relatively tightly coupled to that of the parafoil; the yaw rate data are probably the best indication of turn performance because they are independent of steady winds. Yaw rate data are noisy and must be filtered or curve fit. In this analysis, fourth-order polynomial curve fits were made to yaw rate data turn profiles to determine steady-state turn rates.

Turn rate can also be evaluated by observing heading rate of the velocity vector. Heading rate (HR) is extracted from the wind-corrected velocity data by determining the system heading with respect to east and taking the derivative with respect to time:

$$\text{heading}(t1) = a\tan\left[\frac{V_y(t1)}{V_x(t1)}\right] \tag{16}$$

$$\text{HR}(t2) = \frac{\text{heading}(t2) - \text{heading}(t1)}{(t2 - t1)} \tag{17}$$

Because the difference in atmospheric density at different altitudes, the turn rates are dependent on altitude. Therefore, in the process of analyzing the flight turn rate data, the HR should be corrected to sea level values for proper comparison. An average HR is calculated after the system response has achieved steady state. Figure 18 is an example of a system response to a turn command input. Typical response can be as little as 10 s for small increments in maneuvers (from L0/R0 to L0/R20 %SS) or as long as 20 s for larger maneuvers (from L0/R0 to L0/R60 %SS). Even if short in duration, because the parafoil control stroke slew rate is slow and response dynamics is minimal, what average can be obtained is usually fairly accurate. However, there are instances when the steady-state wind-corrected turn rate does not appear constant. In Fig. 19 the data for

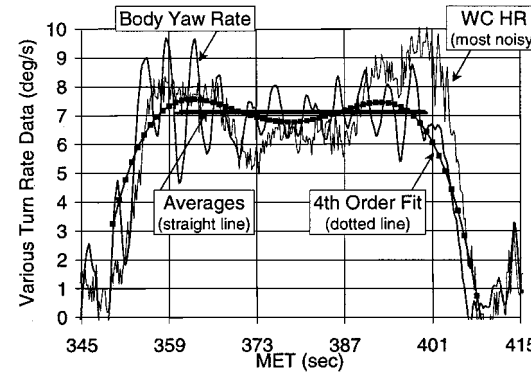

Fig. 19 Example of wind error present during a 360-deg turn (P3D1).

a L50/R70 %SS turn initiating at MET 350 s are plotted. This turn was held long enough for the parafoil to achieve a 360-deg heading change. The observed nonconstant HR is attributed to an error in the wind magnitude estimate because the maneuver traverses a complete 360-deg turn. The fourth-order polynomial curve fit of the HR data suggests that for this full circle maneuver the wind error can be averaged out.

Although turn rates are important for flight planning, it is important to be able to relate them to lateral-directional coefficients for aerodynamic modeling in simulations. Lateral-directional coefficients are also constant for an airfoil and, thus, independent of altitude providing an easier medium with which to analyze. The mechanism for the parafoil turn is unlike that for a conventional aircraft. Rather than the differential flaps inducing a roll angle and subsequent bank maneuver as ailerons would on a conventional aircraft, the difference in drag between the two flaps dictates a yawing motion that causes a turn.[16] In a parafoil's turn maneuver, the yaw moment created by the differential flaps is eventually compensated by the adverse yaw moment (yaw damping) due to the yaw rate. At this point, with constant flap settings achieved, the turn rate reaches a steady state. For each turn rate data point, the quantity $\delta_f Cn_{\delta f}$ was solved for assuming steady state using the following simplified equation[17]:

$$\delta_f Cn_{\delta_f} = \frac{(\text{turn rate})Cn_r b}{2V_{\text{tot}}} \tag{18}$$

Because of limitations in winch performance, the flaps are deflected slowly as compared to similar but smaller personnel parafoil CLD maneuvers. Therefore, the large parafoil's response to turn input is usually nondynamic and remains virtually in steady state throughout the maneuver. With a lack of fast control input and dynamic response, it is inherently difficult to estimate both the flap derivative and the damping derivative. Because of this, Cn_r was assumed constant with a value of 0.0936 for the results presented. Based on analysis of a wide spectrum of turn deflection combinations, $\delta_f Cn_{\delta_f}$ data were curve fit as third-order polynomial functions of delta deflection for various bases (minimum deflected sides). The curves were then interpolated/extrapolated to complete an approximate model for the entire database. The results for rigging angle of 13 deg are presented in Fig. 20.

Discussion of Results

System lift and drag coefficients from several drop tests have been collected as a function of flap deflection and are compiled in Figs. 21 and 22. All results presented pertain to the X-38 5468-ft^2 (508 m^2) parafoil rigged at 13 deg. The system trim C_L and C_D trends of the parafoil are both third-order functions of flap deflection. Initial deflections of the trailing edges provide little change in the aerodynamic performance due to slight dead band or reflex in the control authority. Commanding more flaps tends to increase C_L and C_D, while decreasing lift to drag ratio. As the resulting flight path becomes steeper, the center of pressure moves aft along the parafoil, pitching the parafoil nose down effectively maintaining alpha nearly constant.

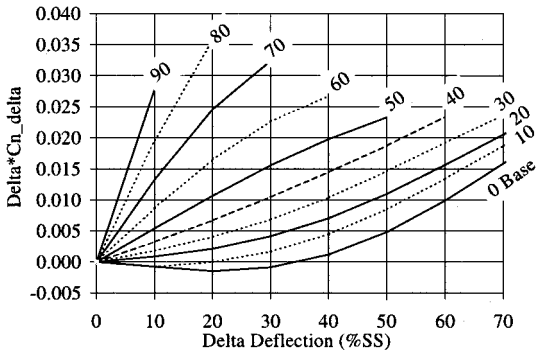

Fig. 20 RA13 $\delta_f Cn_{\delta f}$ database.

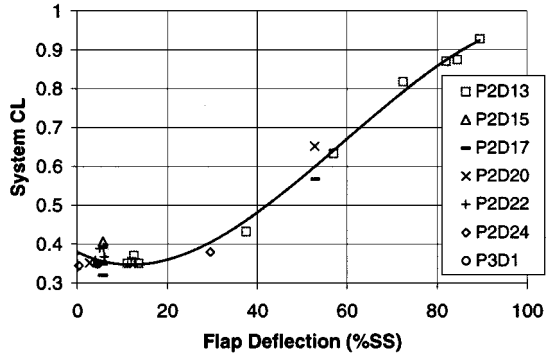

Fig. 21 System C_L flight data collected from phases 2 and 3 testing of 13-deg rigged parafoils.

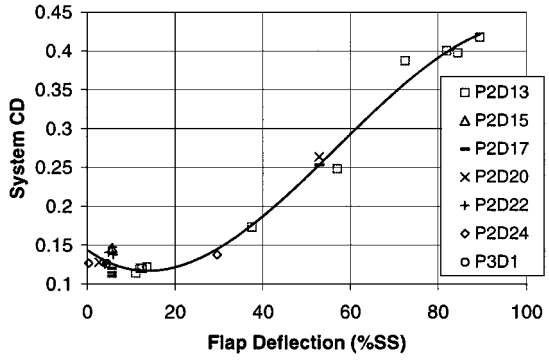

Fig. 22 System C_D flight data from phases 2 and 3 testing of 13-deg rigged parafoils.

The phenomenon called reflex is caused by a chordwise compression of the inflated canopy and manifests itself in the entire span trailing edge deflecting slightly upward while the CLD remains at zero (Fig. 23). This upward deflection of the trailing edge interferes with the flow around the canopy airfoil and, thus, increases drag. A small CLD of the trailing edge flaps removes the reflex on the quarter span associated with the control surface and, consequently, gives the appearance of initially improving canopy performance as demonstrated in Fig. 24. Reflex has been observed frequently in the X-38 large-scale parafoil development program and has caused more of an adverse effect in turn performance.[3] For instance, when a left turn is commanded, initially inputting a left deflection reduces, and eventually removes, the reflex on the left side. Because the upward deflection of the left trailing edge is removed while the right side reflex remains, less drag is induced on the left side of the parafoil than on the right. The result is for the parafoil to turn right while the intent was to turn left, referred to as an adverse turn. Eventually, the left side will be deflected enough to counteract the effect of the reflex on the right side. At this point, the canopy will maintain a constant heading. Further deflection of the left side will finally induce a turn in the left direction; however, the effects of

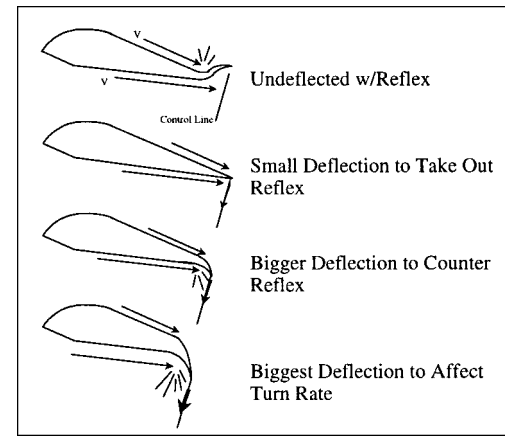

Fig. 23 Description of reflex.

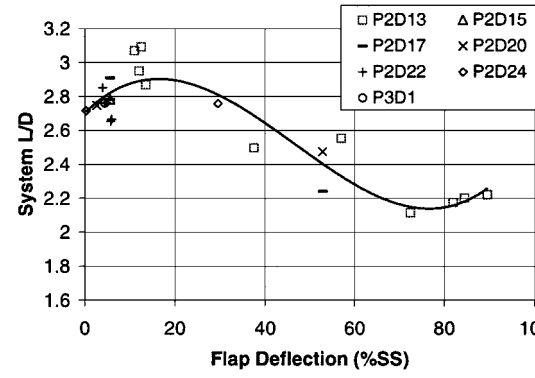

Fig. 24 System lift to drag ratio for a 5468-ft^2 13-deg rigged parafoil.

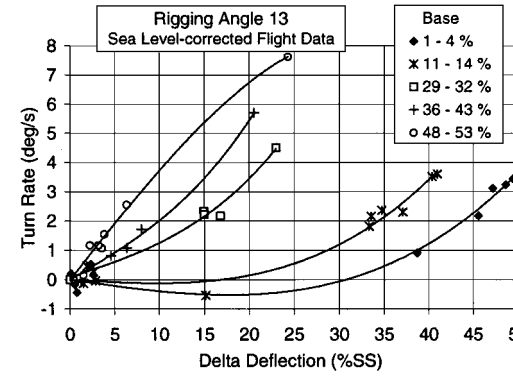

Fig. 25 Third-order polynomial fit of RA13-deg sea-level corrected flight data for various base turns.

reflex are still present on the right side and may cause the turn rate to be lower than predicted. Reflex can be quantified in the parafoil's turn rate model. The negative data points and values of turn rate (adverse turn rate) seen in the 0 base data curve fit are actually the results of reflex. Early in the program, analysts thought these trends and data points were erroneous and were, thus, thrown out. When the model failed to reproduce turn rate trends seen in flight tests, the validity of the negative values were realized, and an updated turn model was created.

Plotting the sea-level corrected turn rate data for a 13-deg rigged canopy as a function of differential CLD for various bases (Fig. 25) allows for many trends to be observed. As already noted, turn rate data are third-order functions of delta deflection for a given base. The knowledge of this characteristic of turn rate data provides for a convenient method of interpolation and extrapolation in the absence of an abundance of data. For a given delta deflection, increasing the base of the turn increases the turn rate. Therefore, if a parafoil

system is flying at 50%SS flaps and the mission requires a turn for range, it is not necessary to back down to a low base just to achieve a big differential to get good turn performance. In actuality, the system can achieve a better turn rate with a smaller delta deflection by further deflecting one of the sides from the 50% flaps. Again referring to Fig. 25, a L50/R0 produces only 3.5 deg/s turn, whereas a L70/R50 turn produces close to 7 deg/s. The parafoil rigged at 10 deg has demonstrated higher turn performance than the parafoil rigged at 13 deg, with similar overall trends. In general, the technique of reducing yaw rate and HR data into aerodynamic coefficients assuming steady-state turns for such a large system with slow inputs works well. Analyzing data as a function of CLD delta for constant base, as well as analyzing data for varying base with constant delta CLD, works well to fill in the gaps in the test database.

Past works have warned of lateral instabilities[16,18] causing spiral divergence. Lingard[16] specifically states that for a parafoil with a span of 30 m (98 ft), a sustained turn rate should be kept less than 11.5 deg/s. X-38 flight data fall in line with this estimate. Spiral divergence has been observed on two occasions during X-38 full-scale testing due to different winch malfunctions. One such occurrence is shown in Figs. 26 and 27. The ground track shown in Fig. 26 shows the severity of the spiral; in particular note the number of complete revolutions completed and the radius of these turns. In Fig. 27, after MET 120, the wind-corrected HR slope steepens marking the point where the turn rate becomes unstable. This corresponds to a command of approximately L75/R5 %SS with a wind-corrected HR between 15 and 18 deg/s. The other flight, P2D23, exhibited similar trends. From these data, the parafoil performance team concluded that spiral divergence for near zero base must occur somewhere around 70%SS. The X-38 program has demonstrated stable steady turn rates for values up to 8 deg/s for periods of up to 45 s at a time (again, see Fig. 19); however, holding a presumed stable differential CLD for more than 360 deg has not been investigated as of yet.

Turn biases can make the evaluation of the parafoil turn performance difficult if not properly identified. Examples of turn bias causes include improper or incomplete inflation of the parafoil, hang-ups in suspension lines or trailing edges, or incorrectly set control lines. In the limited experience of the X-38 program, most turn biases have been less than a 1 deg/s and constant throughout the flight. If any of the aforementioned causes of turn biases are corrected in the middle of the flight, this can remove, or even reverse, the bias and make it even more difficult to discover and assess its effect. Many times the physical cause of a bias is unknown, but its presence can be discovered and evaluated by analyzing turn rates occurring during flap maneuvers as exemplified in Fig. 28. In the case of P2D26, the bias appears to be constant. The success of correcting the data for the bias is demonstrated in Fig. 29. Other times, what may appear to be a turn bias can actually be the effects of reflex.

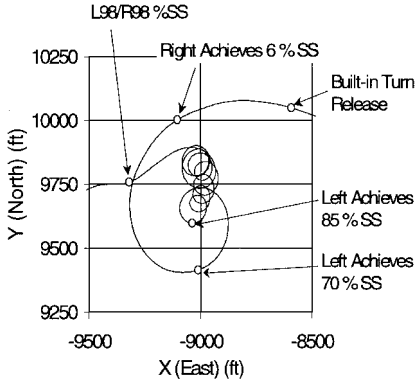

Fig. 26 Example of spiral divergence (P2D21).

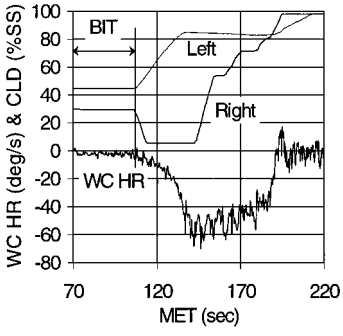

Fig. 27 Example of turn rate induced by spiral divergence (P2D21).

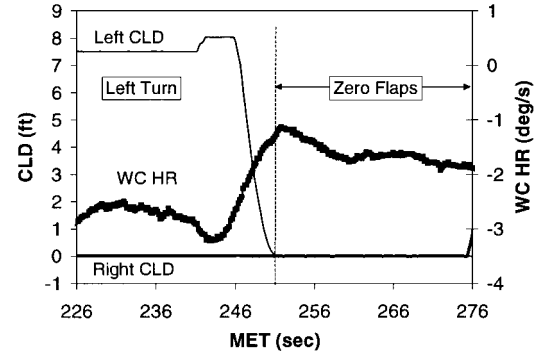

Fig. 28 Example of turn bias (P2D26).

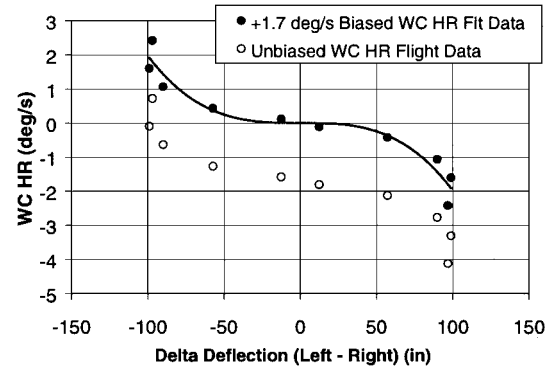

Fig. 29 Applying constant turn bias (P2D26).

Parafoil Dynamic Simulator

Understanding both longitudinal and lateral-directional aerodynamics of a parafoil is critical in supporting development, testing, and implementation of any parafoil-based system. Knowledge of the longitudinal performance is especially helpful when designing test or mission maneuvers. These maneuvers include range safety, energy management to achieve predesignated targets, and flare for optimal landing performance. Knowledge of the turn performance is especially helpful when designing test or mission maneuvers. These maneuvers include hazard avoidance in air or at landing, energy management to achieve predesignated targets, and turns into the wind for optimal landing performance. To demonstrate confidence in this knowledge and to utilize the model operationally, both the longitudinal and lateral-directional aerodynamics were tested and used in simulations both pre- and postflight.

The parafoil dynamic simulator (PDS) is an eight-degree-of-freedom (DOF) simulation that has been developed from previous work under Contract NAS8-36631 for NASA Marshall Space Flight Center. PDS models two-body dynamics where the parafoil rigid body is 6-DOF and the payload rigid body may rotate relative to the parafoil in pitch and yaw. PDS uses the lateral-directional aerodynamic coefficients, Cn_r and $Cn_{\delta f}$, to calculate the yawing moment of the parafoil.[3] PDS also includes longitudinal aerodynamics derived from the X-38 parafoil test program[4] and has been validated by comparison to numerous full-scale drop tests.

Flight Reconstruction: Steady State

Figure 30 provides an example of a PDS trajectory reconstruction. Balloon data were used to make the wind corrections to the

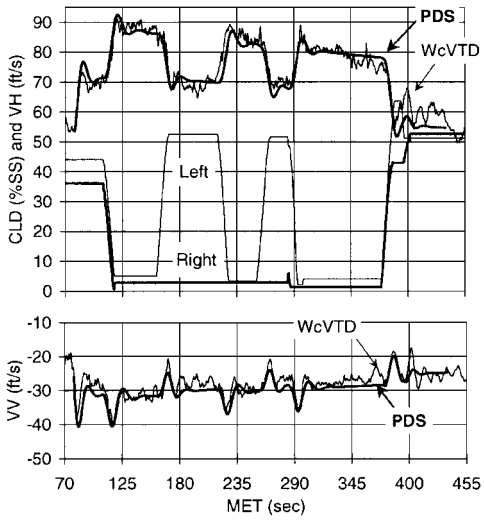

Fig. 30 PDS vs wind-corrected video tracking data (P2D17).

video tracking data because the ADP was not available. PDS was then run without winds for comparison to the wind-corrected flight data. The model currently appears to calculate vertical velocity better in flap maneuvers as opposed to turn maneuvers. For instance, in Fig. 30 during 5%SS flap maneuvers at MET 125 and 235, PDS matches flight data fairly well. However, during turn maneuvers at MET 180 and MET 275, PDS vertical velocities are too high. Currently, PDS assumes the C_L and C_D contributions are averaged between the values for the left and right deflections. Either this is not the correct way to account for C_L and C_D during turn maneuvers or there is some other aspect of the turn model, lateral-directional or longitudinal, that needs to be further investigated. Interestingly enough, horizontal velocities do not appear to have this problem.

There are two other areas of error that are realized in the current modeling. PDS fails to pick up the oscillatory trends seen in vertical velocity that are believed to be of phugoid motion. An example of this motion is seen during both flap and turn maneuvers, in Fig. 30 at MET 125 and 180, respectively. After the aerodynamic database is better defined and verified, analyses of the longitudinal modes will be performed. The other error source shows up more distinctly in horizontal velocity and is attributed to wind uncertainty. During a 5%SS flap maneuver commanded initially around MET 290, PDS horizontal velocities match quite well to the wind-corrected video tracking data. At MET 345, there is a disturbance to the horizontal velocity flight data. The CLDs have not changed, and analysis of the video confirms the canopy is intact. Figure 30 shows a similar anomaly in the vertical velocity flight data at about MET 375. At this time, wind uncertainties, possibly even a vertical gust, are the only explanation offered for this peculiar behavior.

Flight Reconstruction: Longitudinal Dynamic Response

The longitudinal aerodynamics model appears overall to do well in matching dynamic response. Figure 30 demonstrates the PDS model has adequate initial response to flaps inputs. Again, for vertical velocity, the model's dynamic response is better for flap deflections as opposed to turn maneuvers. Note that the response time matches well; however, PDS seems to exhibit slightly lower frequency and higher magnitude in its response. The aerodynamic model is also considered capable of reasonably predicting highly dynamic maneuvers such as flare. The flare maneuver, a full flap defection at the highest retraction rate possible, is performed to reduce quickly vertical and horizontal velocities at touchdown. The X-38 program has tested the flare maneuver at altitude to study the parafoil system's response, and Fig. 31 shows how PDS has been used to reconstruct successfully the maneuver. Recent flights have performed flares at touchdown with a rigging angle of 10 deg, and the data are being analyzed and reconstructed using PDS.

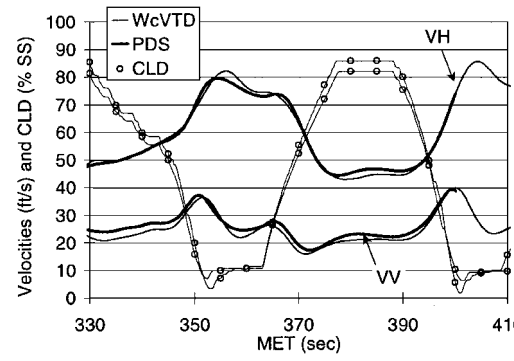

Fig. 31 PDS dynamic reconstruction flare at altitude (P2D13).

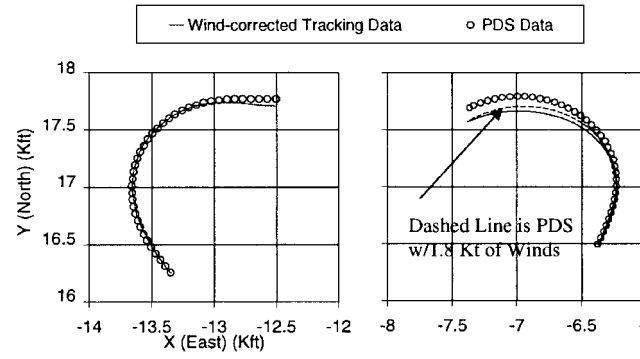

Fig. 32 PDS output compared to flight data for two 0 base turns with 60%SS delta deflection (P2D11).

The general agreement with the flight data trends that are noted in the dynamic response is an indication of the accuracy of the C_L, C_D, and Cm vs alpha slopes. At this time, no modifications have been made to adjust them from the original database, but a method for doing so based on data from both 10- and 13-deg rigged flights is being constructed. Current X-38 drop tests utilize a parafoil rigged at 10 deg rather than 13 deg. Because of the new rigging angle, the parafoil trims at a different alpha.[9] With the current techniques being developed to assess alpha through instrumentation and dynamics comparison as already discussed, the aerodynamic database's alpha slopes will be able to be anchored down between at least two points. These two points are the trim alpha of a 13-deg rigged canopy and its corresponding flight derived C_L, C_D, and Cm and the trim alpha of a 10-deg rigged canopy and its corresponding flight-derived coefficients.

Flight Reconstruction: Lateral-Directional Dynamic Response

When the presented lateral-directional aerodynamic models are used, PDS has been used successfully to reconstruct and predict many X-38 flight tests. PDS and the lateral-directional aerodynamic model can also be implemented to evaluate the quality of the winds collected for a drop. Figure 32 shows the ground track for two zero base turns with delta deflections of 60%SS during the same flight. The first would suggest the PDS model to be correct. The second would suggest PDS to be underperforming. Because PDS can only produce one turn rate for a given turn setting, the difference has been attributed to wind error. After reviewing the wind data and the associated uncertainties for the day, one can usually see that the misalignment between flight data and PDS are within these uncertainties. For the second plot in Fig. 32, PDS was rerun with a constant 1.8 kn (0.9 m/s) out of the north, and the reconstruction match to the flight trajectory is much improved.

Conclusions

The subscale and full-scale phase 2 tests have culminated in the successful development of the primary parachute system for the X-38 atmospheric test vehicles. The concept of using a mortar

deployed decelerator to deploy a parafoil from a lifting body in free flight has been successfully demonstrated. The current parafoil design has repeatedly demonstrated landings with less than 20-ft/s (6.1 m/s) rate of descent. According to the Brinkley analysis of the touchdown loads, these landings have a low probability (less than 0.5% chance) of injuring a deconditioned (due to spending an extended period of time in a weightless environment) and ill or injured human. The lessons and findings from the phase 2 and phase 3 tests will be implemented in the development of the recovery system for the operational CRV.

A method for extracting system longitudinal aerodata from flight-test data for a large-scale parafoil system has been presented. Steady-state maneuvers were analyzed to quantify the parafoil's performance in terms of C_L and C_D as a function of flap deflections by assuming equilibrium glide. Wind corrections to the flight-test trajectory data applied by the ADP or FADS usually gave more consistent results than balloon wind data. It was shown through the compilation of the results that system lift and drag coefficients can both be modeled as third-order functions of flap deflection. Reflex was shown to degrade the performance near zero flaps, but with knowledge of its existence can be properly modeled and accounted for during flight operations. A longitudinal aerodynamic database as a function of alpha was developed to facilitate dynamic analyses and simulations. It was created by maintaining C_L, C_D, and Cm vs alpha slopes compiled from a history of wind-tunnel tests, and applying the flight-derived trim C_L and C_D values at an assumed constant trim angle of attack for each flap setting. Early tow testing analysis, chase video of full-scale parafoil drops, lift distribution analysis, and most recently preliminary parafoil pitch sensor results all suggest the trim alpha to be around 4 deg for a 13-deg rigging angle parafoil. The Cm curves for each flap deflection were anchored by solving for the $Cm_{c/4}$ using the constant trim alpha assumption of 4 deg and the flight-derived C_L and C_D. The longitudinal aeromodel presented herein has been applied to an 8-DOF simulator, which has successfully reconstructed both steady-state and highly dynamic maneuvers. The reasonable dynamic response match between the simulation and flight-test data suggest that the C_L, C_D, and Cm alpha slopes are fairly close. Fortunately, recent testing of large-scale 10-deg rigged parafoils has provided preliminary results capable of defining the slopes and will aid in improving the aerodatabase in future analyses. Further issues to be resolved include the simulation's inadequacy to match vertical velocities during turn maneuvers. This is attributed to incorrect modeling of the turn maneuvers in either the lateral or longitudinal aerodynamics. Another ensuing but minor issue is the simulation's inability to capture an apparent phugoid motion exhibited in the parafoil's vertical velocities. Both are currently being investigated. The end result is an effective method for extracting parafoil longitudinal performance parameters from flight-test data. In addition, this work should allow for a better understanding of large-scale parafoils with a corresponding source of performance data available for comparisons.

The extraction of turn performance and lateral-directional aerodynamics from flight-test data has been successfully demonstrated. Turn performance of the X-38's large-scale parafoil has been efficiently modeled as a third-order function of differential flap deflection for a given base, or minimum deflection. As the base increases, trends also indicate turn rates increase for a given differential CLD. Finally, increasing the rigging angle from 10 to 13 deg decreased turn rates for a given turn setting in inches. Turn biases can be discovered and later quantified by including flap maneuvers in the test objectives. Other undesired adverse turn rates could be attributed to reflex. Techniques for removal of turn biases and modeling of reflex have been demonstrated. Winches capable of fast slew rates are required to estimate the actual yaw-damping coefficient of a large-scale parafoil. However, the X-38 winches, limited to pulling approximately 1.5 ft/s (0.5 m/s), dictate the need for assuming the constant value of Cn_r. Corresponding databases of $Cn_{\delta f}$ for rigging angles of 10 and 13 deg have been presented. Spiral divergence has been observed for both rigging angles of 10 and 13 deg. Subsequently, an attempt has been made to identify the boundary between stable and unstable turn response. The resulting recommendation is to limit near zero base turn maneuvers to a differential deflection of less than 60%SS. Further analysis and testing is needed to address higher bases, as well as the maintenance of turn rate stability for maneuvers held over 360 deg. All of the aforementioned trends and phenomena have been modeled in the 8-DOF parafoil/payload simulator PDS. Flight reconstructions demonstrate the general capability to reproduce observed flight characteristics. One resulting issue that needs to be further investigated is the PDS turn velocities. At this time, both longitudinal aerodynamic calculations for turns and other turn rate parameters are under investigation. Overall, the reader should find this paper to be a valuable source for guidance or comparison in lateral-directional aerodynamic investigations of similar large-scale parafoil systems.

References

[1]Muratore, J., and Iacomini, C., "Parafoil Flight Test of X-38 Prototype Crew Return Vehicle Yields Improved Instrumentation and Techniques," *ITEA Journal of Test and Evaluation*, Vol. 19, No. 2, 1998, pp. 19–24.

[2]Machín, R., Stein, J., and Muratore, J., "An Overview of the X-38 Prototype Crew Return Vehicle Development and Test Program," AIAA Paper 99-1703, June 1999.

[3]Iacomini, C., and Cerimele, C., "Lateral Directional Aerodynamics from a Large Scale Parafoil Test Program," AIAA Paper 99-1731, June 1999.

[4]Iacomini, C., and Cerimele, C., "Longitudinal Aerodynamics from a Large Scale Parafoil Test Program," AIAA Paper 99-1732, June 1999.

[5]Smith, J., and Bennett, T., "Development of the NASA X-38 Parafoil Landing System," AIAA Paper 99-1730, June 1999.

[6]Brinkley, J. W., Specker, L. J., and Mosher, S. E., "Development of Acceleration Exposure Limits for Advanced Escape Systems," AGARD CP Paper 472, April 1989.

[7]Machín, R., Fitzgerald, S., Royall, P., and Walcer, M., "Technique for Measuring Parafoil Deployment and Steady State Loads in the Dispersion Risers and Leading Edge Reinforcement Tape," AIAA Paper 99-1733, June 1999.

[8]Martin, F., "Parafoil Aerodynamic Characteristics Derived from Flight Measured Suspension System Loads," AIAA Paper 99-1734, June 1999.

[9]Iacomini, C., and Madsen, C., "Investigation of Large Scale Parafoil Rigging Angles: Analytical and Drop Test Results," AIAA Paper 99-1752, June 1999.

[10]Bennett, T., Smith, J., and Fox, R., "Testing and Development of the NASA X-38 Parafoil Upper Surface Energy Modulator," AIAA Paper 99-1753, June 1999.

[11]Geiger, R. H., and Golden, R. A., "Pioneer Aerospace Corporation, Advanced Recovery Systems Wind Tunnel Test Report," Rept. ARS-WT-2, Ser. 2, Vol. 1, Pioneer Aerospace Corp., Aug. 1990.

[12]Ware, G. M., and Hassell, J. L., "Wind Tunnel Investigation of Ram-Air-Inflated All-Flexible Wings of Aspect Ratios 1.0 to 3.0," NASA TM SX-1923, Dec. 1969.

[13]Nicolaides, J. D., "Parafoil Wind Tunnel Tests," Rept. AFFDL-TR-70-146, Notre Dame Univ., Notre Dame, IN, June 1971.

[14]Anderson, J. D., Jr., *Fundamentals of Aerodynamics*, 2nd ed., McGraw–Hill, New York, 1984.

[15]Lingard, J. S., "Gliding Parachutes," Parachutes Systems Technology Short Course, Minneapolis, MN, Oct. 1998.

[16]Lingard, J. S., "Ram-Air Parachute Design," 2nd ADS Technology Seminar: Precision Aerial Delivery, May 1995.

[17]Brown, G. J., "Parafoil Steady Turn Response to Control Input," AIAA Paper 93-1241, 1993.

[18]Crimi, P., "Lateral Stability of Gliding Parachutes," *Journal of Guidance, Control, and Dynamics*, Vol. 13, No. 6, 1990, pp. 1060–1063.